ingegneria sismica
International Journal of Earthquake Engineering
Anno XLIII - Num. 2 - 2026

Extraction of Magnetic Gradient Signals from Moving Targets Using High-Tc SQUID Gradiometers

Yixi Zhou[1], *Zhidan Zhang*[1] *and Xiangyan Kong*[1,*]

[1] Institute of Integrated Circuits, Ningbo University 315211, Ningbo, China

SUMMARY: *To address the rapid attenuation of signal amplitude and the difficulty in recovering effective responses under low signal-to-noise ratio (SNR) conditions in long-range detection of moving magnetic targets using high-temperature SQUID planar gradiometers, this study investigates the influence of the relative distance between the target and the sensor on the extractability of magnetic gradient signals. For moving magnetic targets, the Closest Point of Approach (CPA) serves as a key geometric parameter characterizing the minimum distance between the target and the sensor.First, the spatial distribution characteristics of magnetic gradient fields generated by large-scale magnetic targets are analyzed using a COMSOL based finite element model. The results show that as the CPA increases, the lateral coverage of the magnetic gradient disturbance on the observation plane expands, while its peak amplitude decreases significantly. Subsequently, under the condition that the observation distance satisfies the magnetic dipole approximation, a moving magnetic dipole model is established to theoretically analyze the time-domain responses at different CPA. The analysis indicates that, at large CPA, the magnetic gradient signals persist in the form of weak amplitudes with broadened temporal structures. To extract such weak structured signals from noisy measurements, an Orthogonal Basis Functions (OBF) based signal extraction method under a representation normalized with respect to the CPA is introduced. By constructing a structural subspace that matches the response characteristics of the moving magnetic dipole, the proposed method enables structured recovery of magnetic gradient signals under low SNR conditions. Experimental results demonstrate that the proposed method can effectively recover the target response waveform for a magnetic target with a moment of 2.5 A·m² at a maximum distance of approximately 2 m, where the signal approaches the sensitivity limit of the gradiometer, even when the initial SNR is as low as −7 dB. significantly improving signal detectability under weak-signal conditions.The results provide methodological support for the application of high-temperature SQUID planar gradiometers in long-range magnetic anomaly detection.*

KEYWORDS: *High-Tc SQUID planar gradiometer; Magnetic anomaly detection; Closest Point of Approach (CPA) Orthogonal Basis Functions (OBF); Low-SNR signal extraction*

1 Introduction

Detection of moving magnetic targets, as a typical passive sensing approach, has important applications in underwater target detection, concealed object identification, and complex environment perception [1]. In such scenarios, the relative distance between the target and the sensor plays a critical role in determining the spatial distribution and measurability of magnetic anomaly signals. For moving targets, the Closest Point of Approach (CPA) is a key geometric

*18705843612@163.com
https://doi.org/10.65102/is20261036 Published: 30 April, 2026

parameter that characterizes the minimum distance between the target and the sensor, and it has a significant influence on both the amplitude characteristics and spatial distribution of magnetic anomaly signals [2]. With the advancement of magnetic sensing technologies, high-temperature SQUID planar gradiometers, owing to their ultra-high sensitivity and excellent common-mode noise rejection capability[3], have been regarded as a promising tool for long-range magnetic anomaly detection[4]. However, under gradient measurement mode, the magnetic gradient field generated by the target exhibits an approximate fourth-order decay with distance. As a result, with increasing CPA, the signal amplitude decreases rapidly, leading to a significant degradation in signal measurability[5, 6].

The influence of CPA upon abnormal magnetic examination has been comprehensively discussed on theory. Majority of currently existing studies use magnetic dipole approximation and equivalent magnetization models, together with finite element simulation for analyzing the target magnetic field and gradient distribution, hence summarize the changing rule of magnetic gradient amplitude along with CPA. In practical measurement work, magnetic gradient signals undergo sharp decay as CPA increases, and weak long-distance target signals are with great ease submerged by background noise. Although targets may be detected in theory, effective signal characteristics are difficult to draw out in a steady way in actual experiments. Traditional amplitude threshold value judgment and filtering methods cannot keep full target signal characteristics under low SNR, hence they restrict the transformation of theoretical detection effect into actual engineering practice application.

To address the above issue, this work builds upon the analysis of the influence of CPA on both the spatial distribution of magnetic gradient fields and the time-domain responses observed by the sensor, and further focuses on the extraction and recovery of magnetic gradient signals under long-range (large CPA) and low signal-to-noise ratio (SNR) conditions.Based on the structural characteristics of target responses revealed by the moving magnetic dipole model, an Orthogonal Basis Functions (OBF)-based signal extraction method is introduced[11]. The measured magnetic gradient signals are mapped onto a structural subspace constrained by the physical model, where subspace projection and signal reconstruction are employed to effectively suppress noise components that are inconsistent with the target model, thereby achieving stable recovery of the target time-domain gradient response.Unlike conventional approaches that rely on simple amplitude enhancement, the proposed method exploits the consistency of the target magnetic field structure within the subspace to enable structured extraction of weak signals. Experimental results demonstrate that, under weak-signal conditions approaching the sensitivity limit of the gradiometer, the proposed method can significantly improve the recoverability of target responses, providing an effective engineering approach for long-range magnetic anomaly detection using high-temperature SQUID planar gradiometers.

2 Spatial and Temporal Characteristics of Magnetic Gradient Fields

2.1 Spatial Distribution of Magnetic Gradient Fields Under Different CPA

To investigate the detection capability of high-temperature SQUID planar gradiometers for moving magnetic targets under long-range and large-area conditions, it is first necessary to analyze the variation characteristics of the target magnetic gradient field at different observation distances from the perspective of spatial distribution, taking into account the relative position between the sensor and the target [12, 13].Considering that targets in practical applications are often of large size, a large vessel is taken as a representative example and modeled as a triaxial

ellipsoid magnetized by the geomagnetic field[14].Based on this equivalent model, the static magnetic gradient field distribution is calculated using the finite element method. This model ensures physical consistency while effectively capturing the overall spatial structure of the magnetic anomaly gradient field under long-range conditions.

With the increase of CPA, the lateral coverage range of magnetic gradient disturbance expands continuously, while the peak amplitude decreases significantly. This indicates that the signal presents the characteristics of large range and low amplitude under long-distance conditions.

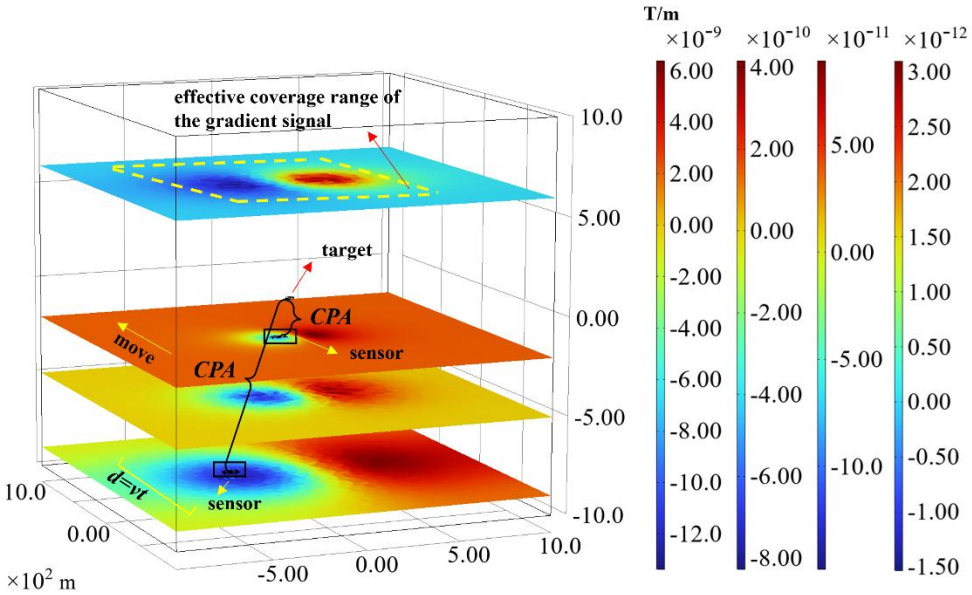

Figure 1: Spatial distribution of magnetic gradient field and effective signal coverage under different CPA conditions

2.2 Time-Domain Width Characteristics of Magnetic Gradient Signals Under Different CPA Conditions

From the analysis of the spatial distribution characteristics of magnetic gradient fields under different CPA conditions, it can be observed that as the CPA increases, the spatial coverage of the magnetic gradient disturbance induced by the target on the observation plane gradually expands, while its amplitude decreases significantly. This indicates that, under long-range conditions, the magnetic anomaly signal exhibits a low-amplitude and widely distributed characteristic in the spatial domain.

The magnetic gradient response generated by a moving target and received by the sensor is typically represented as a time-series signal rather than a purely spatial distribution. Therefore, variations in spatial coverage will inevitably affect the time-domain characteristics of the magnetic gradient signal, particularly its duration and waveform structure.To further reveal the influence of CPA on the time-scale characteristics of magnetic gradient signals, it is necessary to establish a moving magnetic dipole model based on the spatial distribution analysis, describe the relative motion between the target and the sensor, and derive the time-domain response of the magnetic gradient field at the observation point.

When the target size is smaller than 2.5 times the observation distance, the magnetic field generated by the target under the external geomagnetic magnetization can be approximated by a magnetic dipole model[15]. The magnetic moment of the target is defined as:

$$M = M_x\hat{x} + M_y\hat{y} + M_z\hat{z} \tag{1}$$

Taking the gradiometer as the origin, a moving coordinate system is established, as shown in Fig.2(a). The initial position of the target is denoted as(X_0,Y_0,Z_0), and the distance between the target and the gradiometer is R. The magnetic flux density generated by the magnetic dipole at the observation point can be expressed as:

$$B(\vec{R}) = \frac{\mu_0}{4\pi}\left[\frac{3(\vec{M}\cdot\vec{R})\cdot\vec{R}}{R^5} - \frac{\vec{M}}{R^3}\right] \tag{2}$$

The target is assumed to undergo uniform linear motion in the equivalent motion plane. The vertical offset between the sensor and the motion plane is denoted by h, and the vertical displacement is treated as a constant, with $Z(t)=Z_0=-h$.The position vector of the target relative to the sensor is given by:

$$R(t) = \left[X(t), Y(t), Z_0\right]^{\mathrm{T}}, R(t) = \left\|R(t)\right\| = \sqrt{\mathrm{X}^2(t) + \mathrm{Y}^2(t) + \mathrm{Z}_0{}^2} \tag{3}$$

Let v denote the velocity of the target, and let α be the azimuth angle between the direction of motion and the X-axis. The position of the target in the moving coordinate system is given by:

$$\begin{cases} X(t) = v(t - t_0)\cos\alpha \\ Y(t) = Y_0 + v(t - t_0)\sin\alpha \\ Z(t) = Z_0 \end{cases} \tag{4}$$

Denotes the permeability of free space. In the experiment, the gradiometer coils are arranged parallel to the XY plane, with the baseline oriented along the Y-axis. Therefore, the primary measured quantity is the gradient component $G=B_{zy}(\vec{R})=B_{zy}(t)$[16]. During the experiment, the gradiometer remains stationary, while the target moves with a constant velocity of v=0.5m/s along the Y-axis. The time at which the target reaches the closest point to the sensor is denoted as t_0, and the CPA is defined as R_0 . The magnetic moment of the target is given by (0,0,2.5). As shown in Fig.2(b), the magnetic moment is first defined in its local coordinate system and then transformed into the target motion coordinate system O'X'Y'Z' through rotations by angles $\theta_{Mx'}$ and $\theta_{Mz'}$. Substituting the above equations yields:

$$B_{zy}(t) = \frac{3\mu_0}{4\pi}\left[\frac{Z_0 M_y}{R^5(t)} - \frac{5Z_0 Y(t) S(t)}{R^7(t)} + \frac{Y M_z}{R^5(t)}\right] \tag{5}$$

Fig.2(c) shows the projection of CPA and the lateral range during target motion.

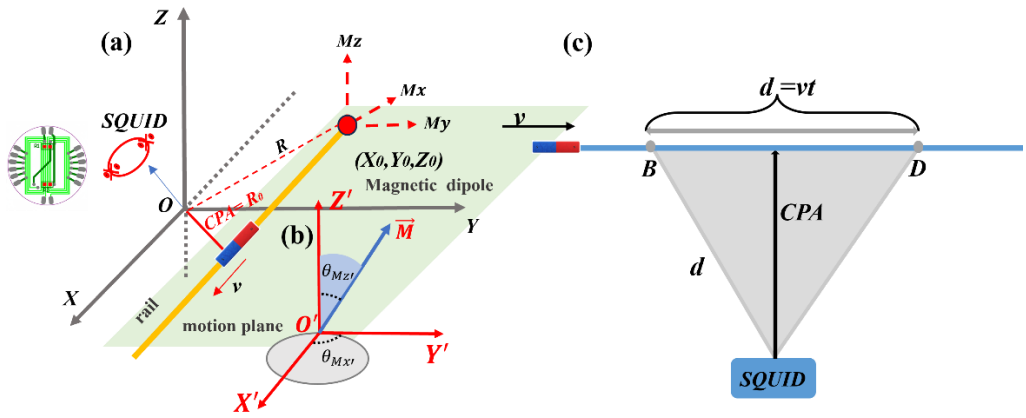

Figure 2: Moving magnetic dipole model: (a) motion coordinate system and key parameters; (b) coordinate transformation of the magnetic moment; (c) projection of CPA and lateral range d.

Based on the time-domain expression of the magnetic gradient derived from (5), numerical simulations are conducted under experimental conditions. By keeping the target velocity and azimuth angle constant, the time-domain signals received by the SQUID gradiometer under different CPA conditions are comparatively analyzed.The outcome of simulation indicates that, when the CPA goes up, the peak amplitude of the magnetic gradient signal becomes smaller, hence its time-domain response displays an obvious widening effect. For the quantitative description of this time-scale change, the full width at half maximum (FWHM) of every signal is got out, and its change with regard to CPA is studied, just like what is shown in Fig.3. The outcome points out that the FWHM grows in one direction along with CPA, which mirrors the time enlargement of the magnetic gradient signal in long-distance situations.

These findings suggest that although the signal amplitude is significantly attenuated with increasing CPA, the intrinsic time-domain structure governed by the physical model is preserved, with variations primarily manifested as changes in the time scale. This provides an important basis for subsequent signal extraction methods based on structural characteristics.

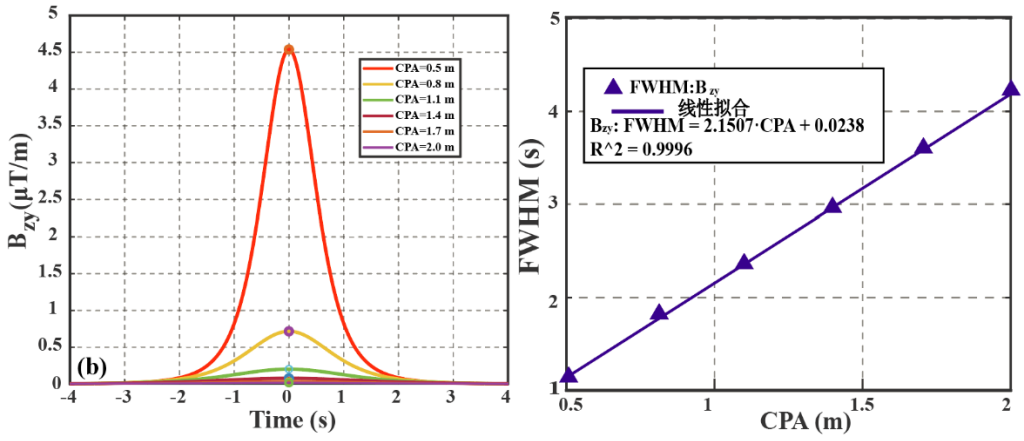

Figure 4: Time-domain responses of magnetic gradient signals and their width variation under different CPA conditions: (a) time-domain waveforms at different CPA values; (b) variation of the full width at half maximum (FWHM) with respect to CPA.

In summary, based on the modeling and simulation analysis of the spatial distribution and time-domain responses of the magnetic gradient field, it is observed that as the CPA increases,

the signal amplitude decreases significantly, while the time-domain response exhibits a pronounced broadening effect. Further analysis indicates that the intrinsic structure of the signal, governed by the physical model, is preserved under varying CPA conditions, with variations primarily manifested as changes in the time scale.These results suggest that, under long-range conditions, the primary challenge in magnetic gradient signal detection arises from the degradation of the signal-to-noise ratio due to amplitude attenuation, rather than the loss of structural information. Therefore, it is necessary to validate these characteristics under practical experimental conditions and to further investigate the sensor response under different CPA scenarios.

This indicates that the structural characteristics of the signal are well preserved, which provides a theoretical basis for structured signal extraction.

3 Experimental System Setup and Testing

To validate the time-domain response characteristics of magnetic gradient signals under different CPA conditions revealed in the previous section, particularly the phenomenon that the signal amplitude significantly attenuates while its intrinsic structure remains preserved under long-range conditions, experiments on magnetic gradient signals generated by a moving magnetic target are conducted. A high-temperature SQUID planar gradiometer-based experimental system is established to enable the measurement and analysis of magnetic gradient signals under low signal-to-noise ratio (SNR) conditions.

The experimental system mainly consists of three components: the SQUID gradiometer detection system, the signal acquisition and control system, and the target motion system, as illustrated in Fig.4. The SQUID gradiometer detection system is used to sense weak magnetic gradient variations induced by the target. The signal acquisition and control system maintains the SQUID in a stable flux-locked loop (FLL) state and converts the gradient signal into a voltage signal for acquisition. The target motion system simulates the motion of the target under different CPA conditions, thereby enabling the acquisition of corresponding time-domain magnetic gradient responses. During the experiment, the gradiometer remains stationary, while the target moves along a predefined trajectory with uniform linear motion. The output signal of the gradiometer is converted by the FLL readout circuit, monitored in real time using an oscilloscope, and transmitted to a host computer via a data acquisition card for storage and subsequent analysis.

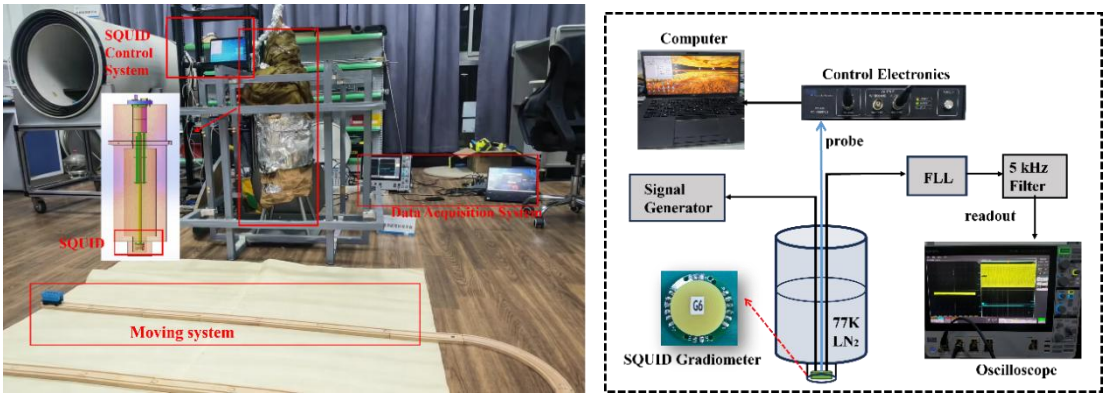

Figure 5: Schematic of the Experimental System

To evaluate the detection capability of the high-temperature SQUID planar gradiometer under weak-signal conditions, the intrinsic gradient sensitivity of the device was characterized,

as shown in Fig.6. The measured gradient noise spectral density is approximately 0.9 nT/(m·√Hz) at 1 Hz, and lies in the range of 0.14–8 nT/(m·√Hz) within the 0.1–10 Hz band. Given the low motion velocity of the target, the dominant spectral energy of the magnetic gradient signal is concentrated in this low-frequency range.

A magnetic target with a moment of 2.5A·m² was used for equivalent experimental validation. By varying the CPA, magnetic gradient responses under different signal strength conditions were acquired. As shown in Fig.7, the signal amplitude decreases markedly with increasing CPA, and approaches the system noise level at approximately 2 m, where the effective signal becomes largely obscured by noise. Although low-pass filtering can attenuate high-frequency noise, it inevitably distorts essential signal characteristics, such as amplitude, peak position, and temporal width, thereby limiting reliable signal recovery.

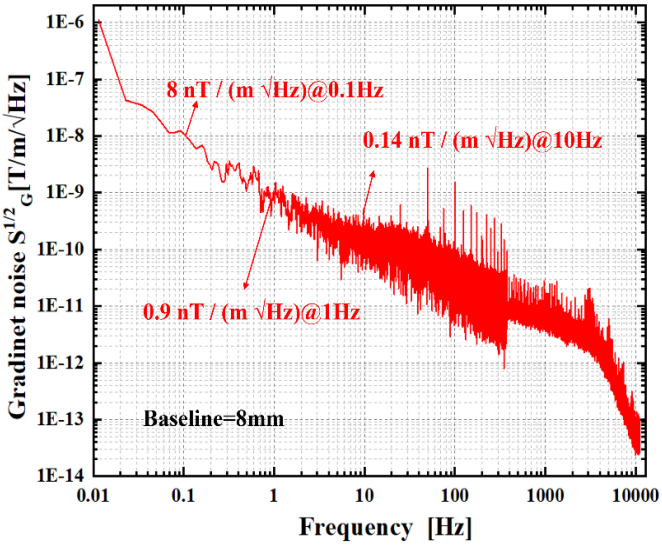

Figure 6: Measured gradient noise spectral density of the SQUID planar gradiometer.

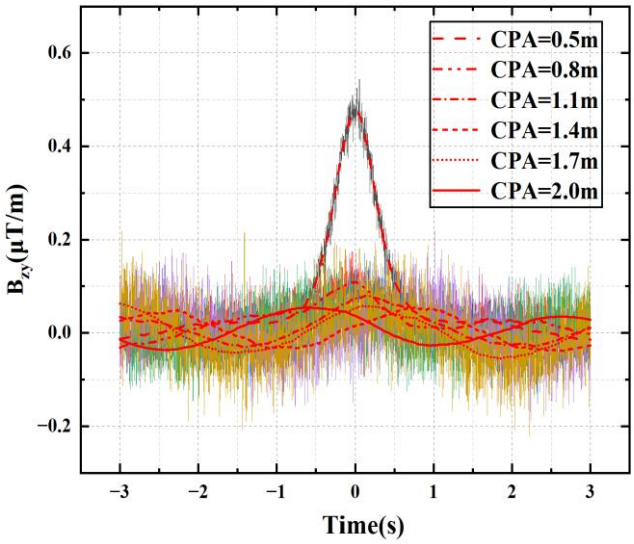

Figure 7: Magnetic gradient signals $B_{zy}(t)$ at different CPA values

As shown in Fig. 7, with increasing CPA, the amplitude of the magnetic gradient signal gradually decreases, while its temporal duration increases, which is consistent with the

simulation results. But, when the CPA go beyond a certain scope, the signal amplitude get close to the system noise level, and a growing part of the effective signal is submerged by noise. Under these circumstances, even though low-pass filtering is able to suppress a portion of high-frequency noises, it hence inevitably brings in distortion effects, which include amplitude attenuation and waveform broadening, therefore it thus lowers the structural features of the signal and hence restricts the obtaining of useful information. Therefore, when the condition of weak signal detection is present, it is necessary that signal processing methods which retain structural features be employed to realize dependable acquisition of magnetic gradient signals.

This system is able to carry out stable measurement on weak magnetic gradient signals, therefore it can provide reliable data support for the extraction of follow-up signals.

4 Structured Extraction of Magnetic Gradient Signals Based on Orthogonal Basis Functions

Under the environments which have low SNR, the core difficult point of magnetic gradient signal processing lies in the separation of weak target signals from a large amount of noise. Although the signals still keep all the physical structure characteristics, traditional filtering and amplitude increasing methods cannot retain this kind of structure information well in the process of noise removing. For the solution of this problem, the present paper puts forward a signal extraction method which is based on OBF. This method has constructed a structural subspace which matches the response characteristics of the moving magnetic dipole, therefore it realizes the stable extraction and high-precision reconstruction of weak target signals.

4.1 OBF Structural Subspace Construction Based on the Moving Magnetic Dipole Model

For the reduction of the effect caused by differences in time and space dimensions in various experiment situations, one no-dimension parameter is brought in by taking t0 as the starting point of phase, in which t0 represents the time moment when the goal arrives at the CPA compared with the sensor, this corresponds to the structure center of the magnetic gradient signal.

$$\omega = \frac{v(t - t_0)}{R_0} \tag{6}$$

Since the actual measurements are obtained through discrete sampling, the measured magnetic gradient signal is denoted as y(t). After baseline removal, it can be expressed as:

$$y_0(t) = y(t) - \bar{y} \tag{7}$$

where $\bar{y}$ is estimated from the mean value of the steady-state segments at the beginning and end of the signal. The baseline-corrected signal $y_0(t)$ is then mapped and interpolated onto a unified dimensionless grid ω_k, denoted as $y_\omega(\omega_k; t_0)$.

In the dimensionless domain, four orthogonal basis functions $g_i(\omega)$, which are consistent with the magnetic gradient response of the moving magnetic dipole, are employed to construct the structural subspace, defined as follows:

$$\begin{cases} g_1(\omega) = \sqrt{\dfrac{1024}{5\pi}} \dfrac{\omega^3}{\left(1+\omega^2\right)^{\frac{7}{2}}} \\ g_2(\omega) = \sqrt{\dfrac{1024}{7\pi}} \dfrac{\omega^2}{\left(1+\omega^2\right)^{\frac{7}{2}}} \\ g_3(\omega) = \sqrt{\dfrac{640}{7\pi}} \left(\dfrac{\omega}{\left(1+\omega^2\right)^{\frac{7}{2}}} - \dfrac{7}{5} \dfrac{\omega^3}{\left(1+\omega^2\right)^{\frac{7}{2}}} \right) \\ g_4(\omega) = \sqrt{\dfrac{128}{21\pi}} \left(\dfrac{1}{\left(1+\omega^2\right)^{\frac{7}{2}}} - 3 \dfrac{\omega^3}{\left(1+\omega^2\right)^{\frac{7}{2}}} \right) \end{cases} \tag{8}$$

where $G(\omega) = \left[g_1(\omega), g_2(\omega), g_3(\omega), g_4(\omega) \right] \in R^{M \times 4}$,These basis functions are derived from the magnetic dipole model and are theoretically orthogonal over an infinite continuous domain. However, under finite windowing and discrete sampling conditions, their orthogonality is only approximately preserved on the discrete ω-grid. To improve the numerical stability of the subsequent coefficient estimation, normalization and numerical orthogonalization, such as the Gram–Schmidt procedure, can be applied to obtain a discrete orthogonal basis, denoted as $\tilde{G}(\omega) = \left[\tilde{g}_1(\omega), \tilde{g}_2(\omega), \tilde{g}_3(\omega), \tilde{g}_4(\omega) \right]$.

On this basis, for each candidate phase origin t_0, the dimensionless signal $y_\omega(\omega_k; t_0)$ is projected onto the structural subspace spanned by $\tilde{G}(\omega)$, and the coefficients are obtained as:

$$a_i(t_0) = \sum_{k=1}^{M} \tilde{g}_i(\omega_k) y_\omega(\omega_k; t_0) \Delta\omega, i = 1,2,3,4 \tag{9}$$

The above process projects the measured signal onto the function subspace spanned by the magnetic dipole response structure, where the coefficients characterize $a_i(t_0)$ the distribution of the signal within this subspace.

Since the phase origin t_0 is unknown in practical measurements, a projection energy is defined as:

$$E(t_0) = \sum_{i=1}^{4} a_i^2(t_0) \tag{10}$$

which characterizes the matching degree between the signal and the structural subspace. When $t_0$coincides with the true closest point of approach (CPA) instant, the signal is best aligned with the basis functions, and the projection energy reaches its maximum. Therefore, the optimal phase origin is determined by:

$$t_0^* = \arg\max_{t_0} E(t_0) \tag{11}$$

Finally, the recovered magnetic gradient signal in the dimensionless domain can be expressed as a linear combination within the OBF structural subspace:

$$\hat{y}_{\omega}(\omega) = \sum_{i=1}^{4} a_i^* \tilde{g}_i(\omega) \tag{12}$$

where $a_i^* = a_i(t_0^*)$ Transforming back to the time domain yields:

$$\hat{y}(t) = \sum_{i=1}^{4} a_i^* \tilde{g}_i\left(\frac{v(t-t_0^*}{R_0}\right) \tag{13}$$

which provides the reconstructed magnetic gradient signal with structural characteristics governed by the magnetic dipole model under a CPA normalized representation.

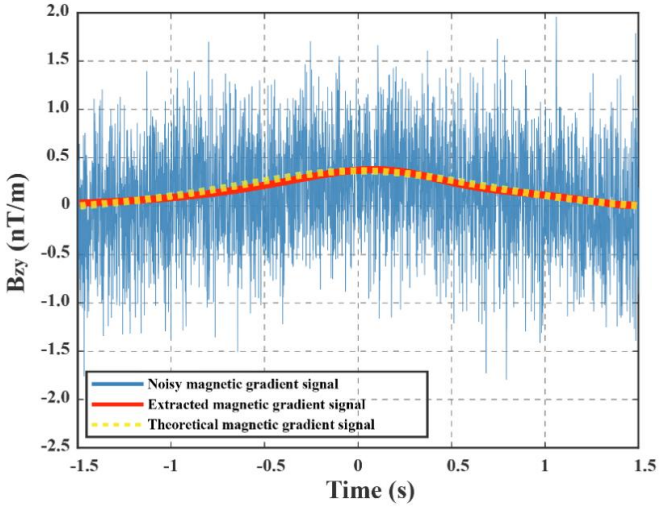

Figure 8: Comparison of noisy, extracted, and theoretical magnetic gradient signals.

To further validate the structural recovery capability of the proposed method, the extracted magnetic gradient signal is compared with the noisy measurement and the theoretical signal, as shown in Fig. 8. It is evident that the reconstructed signal preserves the intrinsic structural characteristics governed by the magnetic dipole model, while effectively suppressing noise components.

This method effectively matches the structural characteristics of moving dipole signals and provides a stable subspace for noise suppression and signal recovery.

4.2 Extraction Performance Evaluation

To quantitatively evaluate the effectiveness of the proposed OBF-based structural extraction method under different CPA conditions, a Signal-to-Noise Ratio (SNR) metric based on energy ratios is introduced. For a given CPA, let the noisy measured magnetic gradient signal be denoted as y(t), the reconstructed signal as $\hat{s}(t)$, and the theoretical reference signal as s(t), which is obtained from the moving magnetic dipole model under the corresponding experimental conditions. The noise and residual components before and after extraction are defined as:

$$\mathrm{n}_{\mathrm{noisy}}(t) = y(t) - s(t), n_{extr} = \hat{s}(t) - s(t) \tag{14}$$

Accordingly, the SNRs before and after extraction are defined as:

$$SNR_{noisy} = 10\log_{10}\left(\frac{\|s(t)\|_2^2}{\|y(t)-s(t)\|_2^2}\right), SNR_{extr} = 10\log_{10}\left(\frac{\|s(t)\|_2^2}{\|\hat{s}(t)-s(t)\|_2^2}\right) \quad (15)$$

Here, SNR_{noisy} characterizes the deviation of the measured signal from the theoretical structural response, while SNR_{extr} reflects the capability of the proposed method to recover the target signal structure. The SNR improvement is further defined as:

$$\Delta SNR = SNR_{extr} - SNR_{noisy} \quad (16)$$

Based on these definitions, the variations of, SNR_{noisy}, SNR_{extr} and ΔSNR with respect to CPA are evaluated. As shown in Fig. 9(a), with increasing CPA, the SNR of the original measured signal decreases rapidly and eventually approaches −7 dB at larger distances, indicating that the target response becomes severely submerged in noise. In contrast, the extracted signal maintains a significantly higher SNR over a wide range of CPA values, demonstrating the effectiveness of the proposed method in recovering the structural characteristics of the magnetic gradient signal under low SNR conditions.

Fig. 9(b) presents the variation of ΔSNR as a function of CPA. At smaller CPA values, the original signal already exhibits a relatively high SNR, and thus the improvement achieved by the proposed method is limited, resulting in a small ΔSNR. As CPA increases, the SNR of the original signal deteriorates rapidly, while the advantage of the OBF-based structural extraction becomes increasingly prominent. Consequently, rises ΔSNR significantly and remains at a high level in the mid-to-long range. These outcome show that the method which we put forward is especially good at getting back weak magnetic gradient signals under the situation of large CPA and low SNR, therefore thus it greatly raises the degree that people can detect signals. Beside the quantitative promotion of SNR, the comparison of waveform that is shown in Fig.8 further proves that the reconstructed signal possesses good consistency with the theoretical reference on aspects of peak position, whole shape and time expansion. This therefore proves that the method we put forward not only can restrain noise but also can effectively keep the original inner structure features of the magnetic gradient signal.

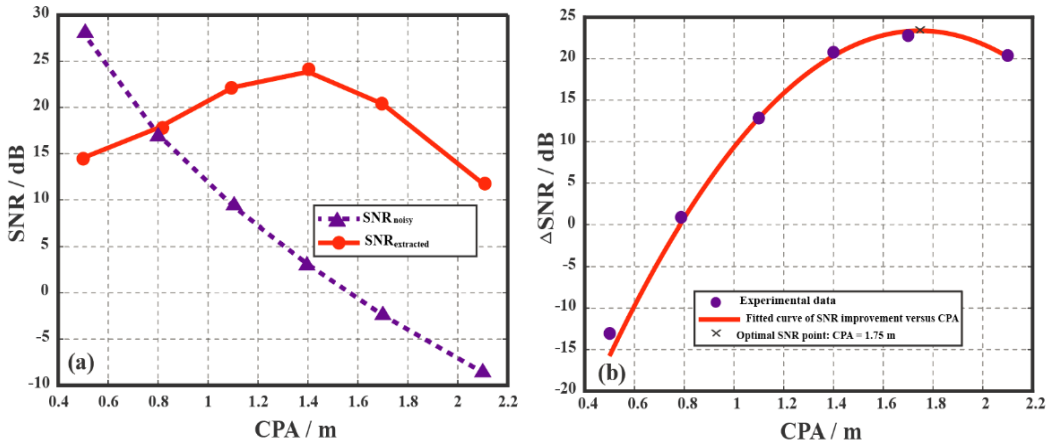

Figure 9: SNR performance evaluation of the OBF-based extraction method under different CPA conditions. (a) SNR comparison before and after extraction versus CPA; (b) SNR improvement ΔSNR versus CPA and its fitted curve, showing enhanced performance at larger CPA values.

On the whole, the extraction performance examination has confirmed the useful effect of the put-forward method in obtaining weak structured magnetic gradient signals under different CPA conditions, especially in middle-to-long distance detection situations, therefore giving quantitative support for the following analysis of long-distance magnetic anomaly detection ability.

5 Conclusion

This article systematically makes a research on the effect of CPA on the space distribution and time domain characteristics of magnetic gradient signals which come from moving magnetic objects. Along with the rising of CPA, the amplitude of the signal experiences an obvious decrease, and the time-domain waveform becomes wider, while the inherent physical structure characteristics of it still do not change. For the extraction of weak signals under the condition of large CPA and low SNR, this paper therefore puts forward a structured signal extraction method of CPA normalization which is based on orthogonal basis functions. It makes signals of different CPA map to a unified no-dimension domain, constructs a matched structure subspace, hence realizes stable signal reconstruction through phase alignment and projection energy maximization. Experimental outcome confirms that this method is able to effectively retrieve target wave shapes under low SNR of minus 7 dB and a CPA of two meters, and thus greatly promote the SNR of medium and long distance detection.

These outcome show the method we put forward can effectively keep the structure features of magnetic gradient signals in weak signal situations, and therefore provide a dependable method for long-distance magnetic abnormal examination that uses high-temperature SQUID plane gradiometers.

Funding

This work was supported by National Key Science and Technology Project for Deep Earth Exploration and Mineral Resources Investigation (Grant No. 2024ZD1002700).

About The Author

Yixi Zhou (2000–), Female, Chengdu, Sichuan, China, M.S. candidate. Research interests: magnetic sensors and their applications. 2311100037@nbu.edu.cn

Zhidan Zhang (1996–), male, Ningbo, Zhejiang, China, Ph.D. Candidate Research interests: magnetic sensors and their applications. Zhangzhidan@nbu.edu.cn

Xiangyan Kong (1973–), Female, Female, Shanghai, China, Professor. Research interests: intelligent sensing and quantum precision measurement. 18705843612@163.com

References

[1] H. Zhang and M. Y. Xia, “Magnetic anomaly detection for simultaneous moving target and magnetometer,” in *Proc. 3rd Asia-Pacific Conf. Antennas and Propagation*, 2014, pp. 884–888.

[2] C. Chi, D. Wang, Z. Yu, *et al.*, "A hybrid method for positioning a moving magnetic target and estimating its magnetic moment," *IEEE Sensors Journal*, vol. 23, no. 21, pp. 25882–25894, 2023.

[3] Y. Shen, D. Hasanyan, J. Q. Gao, *et al.*, "A magnetic signature study using magnetoelectric laminate sensors," *Smart Materials and Structures*, vol. 22, no. 9, 2013.

[4] D. G. Liu, X. Xu, C. J. Fei, *et al.*, "Direction identification of a moving ferromagnetic object by magnetic anomaly," *Sensors and Actuators A: Physical*, vol. 229, pp. 147–153, 2015.

[5] Y. Shen, J. Z. Wang, J. D. Shi, *et al.*, "Interpretation of signature waveform characteristics for magnetic anomaly detection using tunneling magnetoresistive sensor," *Journal of Magnetism and Magnetic Materials*, vol. 484, pp. 164–171, 2019.

[6] C. P. Du, M. Y. Xia, S. X. Huang, *et al.*, "Detection of a moving magnetic dipole target using multiple scalar magnetometers," *IEEE Geoscience and Remote Sensing Letters*, vol. 14, no. 7, pp. 1166–1170, 2017.

[7] T. Nara, S. Suzuki, and S. Ando, "A closed-form formula for magnetic dipole localization by measurement of its magnetic field and spatial gradients," *IEEE Transactions on Magnetics*, vol. 42, no. 10, pp. 3291–3293, 2006.

[8] J. Zhang, C. S. Lin, P. Deng, *et al.*, "Magnetic anomaly signal detection algorithm based on wavelet-domain OBF decomposition," *Journal of Projectiles, Rockets, Missiles and Guidance*, vol. 31, no. 6, pp. 187–189, 2011.

[9] Y. Q. Zhang and S. C. Mao, "Modeling and analysis of submarine magnetic field and its application," *Ship Electronic Engineering*, vol. 38, no. 1, pp. 136–139, 2018.

[10] Y. Wang, Q. Fu, and Y. Y. Sui, "A robust tracking method for multiple moving targets based on equivalent magnetic force," *Micromachines*, vol. 13, no. 11, 2022.

[11] J. F. Ma, B. Yan, and C. S. Lin, "Vector magnetic gradient anomaly detection based on orthogonal basis functions," *Acta Armamentarii*, vol. 42, no. 11, pp. 2433–2443, 2021.

[12] H. Yin, X. Wen, S. S. Yang, *et al.*, "Research on identification method of moving magnetic targets based on magnetic anomaly detection," *Chinese Journal of Scientific Instrument*, vol. 39, no. 3, pp. 258–264, 2018.

[13] S. Nazlibilek, Y. Ege, and O. Kalender, "A multi-sensor network for direction finding of moving ferromagnetic objects inside water by magnetic anomaly," *Measurement*, vol. 42, no. 9, pp. 1402–1416, 2009.

[14] H. Liu, "Magnetic anomaly calculation model of submarine based on induced magnetic field," *Journal of Unmanned Undersea Systems*, vol. 26, no. 2, pp. 152–156, 2018.

[15] Z. C. Yang, S. K. Li, X. Da, *et al.*, "Robust online compensation and magnetic anomaly detection on a rotating platform with three-axis magnetometers," *IEEE Transactions on Geoscience and Remote Sensing*, vol. 63, 2025.

[16] M. Luo, Z. H. Xu, J. X. Pei, *et al.*, “A tracking approach of a moving ferromagnetic object using triaxial search coil data,” *IEEE Transactions on Geoscience and Remote Sensing*, vol. 62, 2024.